

# Exclusive photoproduction of $J/\psi$ in proton-proton and proton-antiproton scattering

W. Schäfer<sup>1,\*</sup> and A. Szczurek<sup>1,2,†</sup>

<sup>1</sup>*Institute of Nuclear Physics PAN, PL-31-342 Cracow, Poland*

<sup>2</sup>*University of Rzeszów, PL-35-959 Rzeszów, Poland*

(Dated: February 5, 2008)

## Abstract

Protons and antiprotons at collider energies are a source of high energy Weizsäcker–Williams photons. This may open a possibility to study exclusive photoproduction of heavy vector mesons at energies much larger than possible at the HERA accelerator. Here we present a detailed investigation of the exclusive  $J/\psi$  photoproduction in proton-proton (RHIC, LHC) and proton-antiproton (Tevatron) collisions. We calculate several differential distributions in  $t_1, t_2, y, \phi$ , as well as transverse momentum distributions of  $J/\Psi$ 's. We discuss correlations in the azimuthal angle between outgoing protons or proton and antiproton as well as in the  $(t_1, t_2)$  space. Differently from electroproduction experiments, here both colliding beam particles can be a source of photons, and we find large interference terms in azimuthal angle distributions in a broad range of rapidities of the produced meson. We also include the spin–flip parts in the electromagnetic vertices. We discuss the effect of absorptive corrections on various distributions. Interestingly, absorption corrections induce a charge asymmetry in rapidity distributions, and are larger for  $pp$  reactions than for the  $p\bar{p}$  case. The reaction considered here constitutes an important nonreduceable background in recently proposed searches for odderon exchange.

*dedicated to Kolya Nikolaev on the occasion of his 60th birthday*

PACS numbers: 13.87.Ce, 13.60.Le, 13.85.Lg

---

\*Electronic address: Wolfgang.Schafer@ifj.edu.pl

†Electronic address: Antoni.Szczurek@ifj.edu.pl

## I. INTRODUCTION

The diffractive photoproduction of  $J/\psi$ -mesons has been recently a subject of thorough studies at HERA [1, 2], and serves to elucidate the physics of the QCD pomeron and/or the small- $x$  gluon density in the proton (for a recent review and references, see [3]). Being charged particles, protons/antiprotons available at e.g. RHIC, Tevatron and LHC are a source of high energy Weizsäcker–Williams photons, and photoproduction processes are also accessible in hadronic collisions. Hadronic exclusive production mechanisms of mesons at central rapidities in  $pp$  collisions were intensively studied in the 1990-ies at energies of a few tens of GeV [4], and raised much theoretical interest for their potential of investigating exotic hadronic states (see e.g. [5]). Recently there was interest in describing diffractive exclusive production of heavy scalar [6, 7] and pseudoscalar [8] mesons in terms of off-diagonal unintegrated gluon distributions, which may provide insight into the related diffractive production mechanism of the Higgs boson ([9, 10] and references therein). A purely hadronic mechanism for the exclusive production of  $J/\Psi$  mesons in proton-proton and proton-antiproton collisions was suggested as a candidate in searches for yet another exotic object of QCD, the elusive odderon exchange [11, 12]. In order to identify the odderon exchange one has to consider all other possible processes leading to the same final channel which in the context of the searches for the odderon will constitute the unwanted background. One of such processes (and perhaps the only one at the level of fully exclusive  $J/\Psi$ -production) is pomeron-photon or photon-pomeron fusion [12, 13, 14], which we study in this communication at a more detailed level than available in the literature. We feel that its role as a background for odderon searches warrants a more detailed analysis including energy dependence and differential distributions of the photoproduction mechanism in hadronic collisions. As will be discussed, the process considered here is interesting also in its own rights.

An important concern of our work are absorption effects. More often than not absorption effects are either completely ignored or included as a multiplicative reduction factor, which is simply wrong for many observables (like distributions in  $t_1$  or  $t_2$ ) as we shall show in our paper. We think this point requires broader public spread as it often appears to be forgotten or ignored. We present a detailed analysis of several differential distributions in order to identify the absorption effects. We also put a special emphasis on interference phenomena. We will discuss also more subtle phenomena like the spin flip in the electromagnetic vertices and a charge asymmetry by comparing differential distributions in proton-proton and proton-antiproton exclusive  $J/\psi$  production.

In this work, we do not include a possible odderon contribution. We wish to stress, that the photoproduction mechanism of exclusive  $J/\Psi$ 's must exist without doubt, and does not die out as energy increases. A related purely hadronic (Odderon) contribution with the same properties has not been unambiguously identified in other experiments, and hence cannot be estimated in a model-independent way. While certain QCD-inspired toy-models for CP-odd multigluon t-channel exchanges exist, they do not allow reliable calculations of hadronic amplitudes. In practice the magnitude of the corresponding Born amplitude strongly depend on the details of how to treat gluons in the nonperturbative domain, as well as on the modeling of proton structure. Furthermore, the energy dependence of the full (beyond the Born approximation, and beyond perturbation theory) amplitude is unknown and it can even not be excluded that this contribution would vanish with rising energy. It is not the issue of our paper to further discuss such models, we rather think that in the search for an odderon one should take further initiative, if substantial deviations from the more

conservative physics discussed here are found.

## II. AMPLITUDES AND CROSS SECTIONS

### A. $2 \rightarrow 3$ amplitude

Here we present the necessary formalism for the calculation of amplitudes and cross-sections. The basic mechanisms are shown in Fig.1.

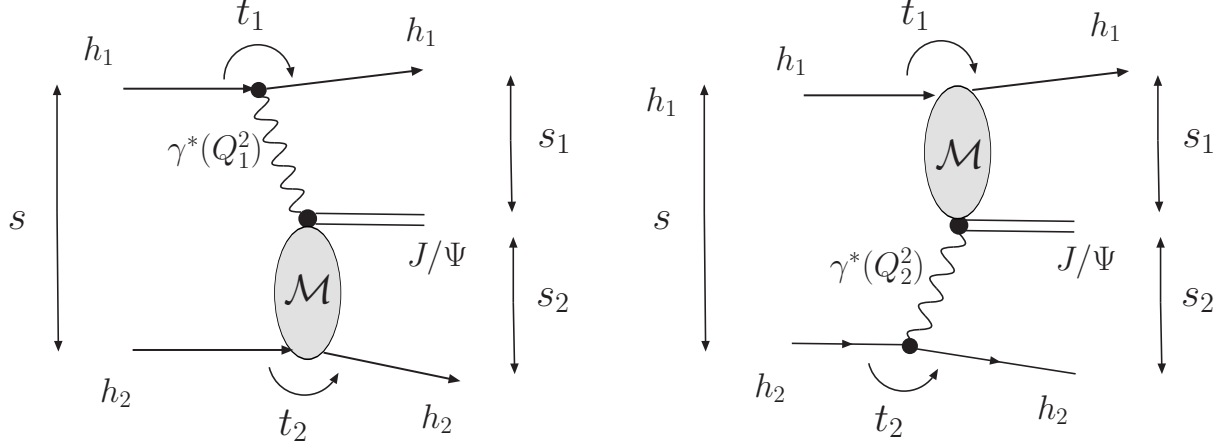


FIG. 1: The sketch of the two mechanisms considered in the present paper:  $\gamma\mathbf{IP}$  (left) and  $\mathbf{IP}\gamma$  (right). Some kinematical variables are shown in addition.

The distinctive feature, when compared to photoproduction in lepton-hadron collisions, is that now both participating hadrons can serve as the source of the photon, and it is necessary to take account of the interference between the two amplitudes. Due to the Coulomb singularities in the photon exchange parts of the amplitude, the electromagnetic vertices involve only very small, predominantly transverse momentum transfers. Their effect is fully quantified by the well-known electromagnetic Dirac- and Pauli form factors of the nucleon. Regarding the photoproduction amplitude, we try to be as far as possible model independent, and take advantage of the precise knowledge of diffractive vector meson production over a broad energy range available from experiments at HERA. The amplitude for the  $2 \rightarrow 3$  process of Fig.1 can be decomposed as

$$\begin{aligned}
 \mathcal{M}_{h_1 h_2 \rightarrow h_1 h_2 V}^{\lambda_1 \lambda_2 \rightarrow \lambda'_1 \lambda'_2 \lambda_V}(s, s_1, s_2, t_1, t_2) &= \mathcal{M}_{\gamma\mathbf{IP}} + \mathcal{M}_{\mathbf{IP}\gamma} \\
 &= \langle p'_1, \lambda'_1 | J_\mu | p_1, \lambda_1 \rangle \epsilon_\mu^*(q_1, \lambda_V) \frac{\sqrt{4\pi\alpha_{em}}}{t_1} \mathcal{M}_{\gamma^* h_2 \rightarrow V h_2}^{\lambda_{\gamma^*} \lambda_2 \rightarrow \lambda_V \lambda_2}(s_2, t_2, Q_1^2) \\
 &\quad + \langle p'_2, \lambda'_2 | J_\mu | p_2, \lambda_2 \rangle \epsilon_\mu^*(q_2, \lambda_V) \frac{\sqrt{4\pi\alpha_{em}}}{t_2} \mathcal{M}_{\gamma^* h_1 \rightarrow V h_1}^{\lambda_{\gamma^*} \lambda_1 \rightarrow \lambda_V \lambda_1}(s_1, t_1, Q_2^2).
 \end{aligned} \tag{2.1}$$

The outgoing protons lose only tiny fractions  $z_1, z_2 \ll 1$  of their longitudinal momenta. In terms of their transverse momenta  $\mathbf{p}_{1,2}$  the relevant four-momentum transfers squared are  $t_i = -(\mathbf{p}_i^2 + z_i^2 m_p^2)/(1 - z_i)$ ,  $i = 1, 2$ , and  $s_1 \approx (1 - z_2)s$  and  $s_2 \approx (1 - z_1)s$  are the

familiar Mandelstam variables for the appropriate subsystems. Due to the smallness of the photon virtualities, denoted by  $Q_i^2 = -t_i$ ,<sup>1</sup> it is justified to neglect the contribution from longitudinal photons, recall that  $\sigma_L(\gamma^*p \rightarrow J/\Psi p)/\sigma_T(\gamma^*p \rightarrow J/\Psi p) \propto Q^2/m_{J/\Psi}^2$  [2, 3]. Then, the amplitude for emission of a photon of transverse polarization  $\lambda_V$ , and transverse momentum  $\mathbf{q}_1 = -\mathbf{p}_1$ , entering eq.(2.1) reads:

$$\langle p'_1, \lambda'_1 | J_\mu | p_1, \lambda_1 \rangle \epsilon_\mu^*(q_1, \lambda_V) = \frac{(\mathbf{e}^{*(\lambda_V)} \mathbf{q}_1)}{\sqrt{1-z_1}} \frac{2}{z_1} \chi_{\lambda'}^\dagger \left\{ F_1(Q_1^2) - \frac{i\kappa_p F_2(Q_1^2)}{2m_p} (\boldsymbol{\sigma}_1 \cdot [\mathbf{q}_1, \mathbf{n}]) \right\} \chi_\lambda, \quad (2.2)$$

here  $\mathbf{e}^{(\lambda)} = -(\lambda \mathbf{e}_x + i \mathbf{e}_y)/\sqrt{2}$ ,  $\mathbf{n} \parallel \mathbf{e}_z$  denotes the collision axis, and  $\boldsymbol{\sigma}_1/2$  is the spin operator for nucleon 1,  $\chi_\lambda$  is its spinor.  $F_1$  and  $F_2$  are the Dirac- and Pauli electromagnetic form factors, respectively. Here we have given only that part of the current, which gives rise to the logarithmic  $dz/z$  longitudinal momentum spectrum of photons, which dominates in the high-energy kinematics considered here. It is worthwhile to recall, that for a massive fermion, that includes a spin-flip contribution originating from its anomalous magnetic moment,  $\kappa_p = 1.79$ . Notice its suppression at small transverse momenta. The parametrization of the photoproduction amplitude which we used in practical calculations can be found in the Appendix. Above we already used the assumption of  $s$ -channel-helicity conservation in the  $\gamma^* \rightarrow J/\Psi$  transition, which for heavy vector mesons is indeed well justified by experiment<sup>2</sup> [1, 2, 3]. In summary we present the  $2 \rightarrow 3$  amplitude in the form of a 2-dimensional vector as

$$\begin{aligned} \mathbf{M}(\mathbf{p}_1, \mathbf{p}_2) &= e_1 \frac{2}{z_1} \frac{\mathbf{p}_1}{t_1} \mathcal{F}_{\lambda'_1 \lambda_1}(\mathbf{p}_1, t_1) \mathcal{M}_{\gamma^* h_2 \rightarrow V h_2}(s_2, t_2, Q_1^2) \\ &+ e_2 \frac{2}{z_2} \frac{\mathbf{p}_2}{t_2} \mathcal{F}_{\lambda'_2 \lambda_2}(\mathbf{p}_2, t_2) \mathcal{M}_{\gamma^* h_1 \rightarrow V h_1}(s_1, t_1, Q_2^2). \end{aligned} \quad (2.3)$$

The differential cross section of interest is given in terms of  $\mathbf{M}$  as

$$d\sigma = \frac{1}{512\pi^4 s^2} |\mathbf{M}|^2 dy dt_1 dt_2 d\phi, \quad (2.4)$$

where  $y \approx \log(z_1 \sqrt{s}/m_{J/\Psi})$  is the rapidity of the vector meson, and  $\phi$  is the angle between  $\mathbf{p}_1$  and  $\mathbf{p}_2$ . Notice that the interference between the two mechanisms  $\gamma \mathbf{IP}$  and  $\mathbf{IP} \gamma$  is proportional to  $e_1 e_2 (\mathbf{p}_1 \cdot \mathbf{p}_2)$  and introduces a charge asymmetry as well as an angular correlation between the outgoing protons. Clearly, the interference cancels out after integrating over  $\phi$ , and the so integrated distributions will coincide for  $pp$  and  $p\bar{p}$  collisions.

## B. Absorptive corrections

We still need to correct for a major omission in our description of the production amplitude. Consider for example a rest frame of the proton 2 (the target) of the left panel of Fig 1. Here, the virtual photon may be viewed as a parton of proton 1 (the beam), separated from

<sup>1</sup> Of course here the notation  $Q_i^2 = t_i$  applies only to the photon lines.

<sup>2</sup> While a trend towards  $s$ -channel helicity violating effects may be visible in the H1 data [2], they are surely negligible for our purpose, and within error bars, consistent with [1] and  $s$ -channel helicity conservation.

it by a large distance in impact parameter space. It splits into its  $c\bar{c}$ -Fock component at a large longitudinal distance before the target, and to obtain the sought for production amplitude we project the elastically scattered  $c\bar{c}$  system onto the desired  $J/\Psi$ -final state [15]. We entirely neglected the possibility [16] that the photon's spectator partons might participate in the interaction, and destroy the rapidity gap(s) in the final state. Stated differently, for the diffractive final state of interest, spectator interactions do not cancel, and will affect the cross section. As a QCD-mechanism consider the interaction of a  $\{c\bar{c}\}_1\{qqq\}_1$ -beam system with the target by multiple gluon exchanges (see Fig 2 ). Then, for the  $J/\Psi$  final state

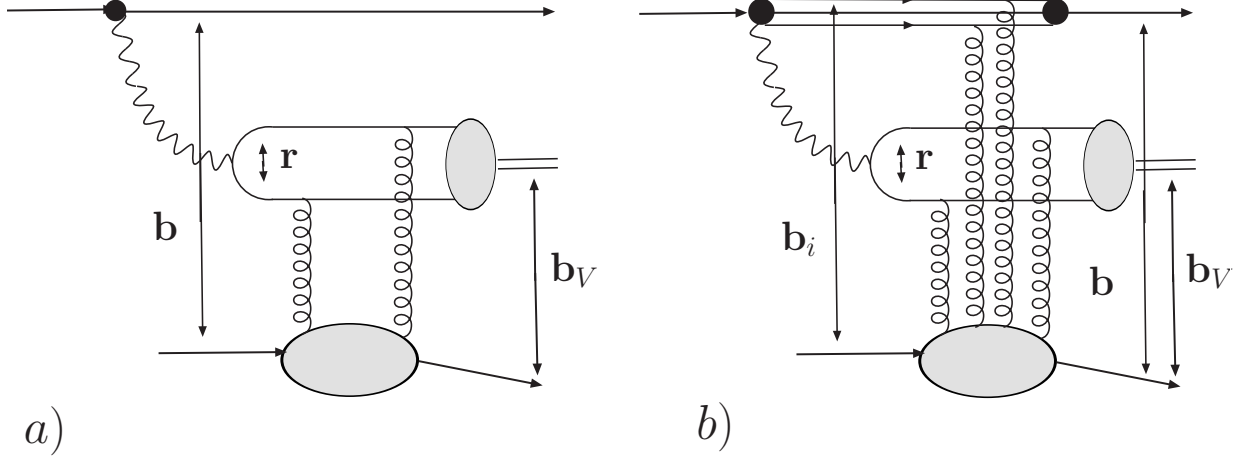


FIG. 2: Left: the QCD two-gluon exchange mechanism for the Born-level amplitude. Right: a possible multigluon-exchange contribution that involves uncancelled spectator interactions. The impact parameters relevant for the discussion are indicated.

of interest, the interaction of the  $c\bar{c}$ -color singlet state is dominated by small dipole sizes  $r_s \sim 4/m_{J/\Psi}$  (the scanning radius of [17]). It can be exhausted by the minimal two-gluon color-singlet exchange, and will be quantified by the color-dipole cross section  $\sigma(\mathbf{r})$  [15, 18], respectively its non-forward generalization [19, 20]. Let  $\mathbf{b}_V$  be the transverse separation of the  $J/\Psi$  and the target, and  $\mathbf{r}$  the size of the  $c\bar{c}$ -dipole as shown in Fig 2. Then, the  $2 \rightarrow 3$  amplitude of section II A will involve, besides the vertex for the  $p \rightarrow \gamma p$  transition, the expectation value  $\langle J/\Psi | \Gamma^{(0)}(\mathbf{r}, \mathbf{b}_V) | \gamma \rangle$  of

$$\Gamma^{(0)}(\mathbf{r}, \mathbf{b}_V) = \frac{1}{2} \sigma(\mathbf{r}) t_N(\mathbf{b}_V, B), \quad (2.5)$$

where  $t_N(\mathbf{b}, B) = \exp(-\mathbf{b}^2/2B)/(2\pi B)$  is an optical density of the target. Systematic account for the spectator interactions in QCD however is a difficult problem, as one cannot rely on the Abramovsky-Gribov-Kancheli (AGK) [21] cutting rules, when due account for color is taken [22]. To obtain at least a qualitative account of absorptive corrections we restrict ourselves to only a subclass of absorptive corrections, the 'diffractive cut', which contribution is model independent [23]. Regarding our  $\{c\bar{c}\}_1\{qqq\}_1$ -system, with  $\mathbf{b}_i$  denoting the constituent quarks' impact parameters, and  $\mathbf{b}$  the impact parameter of the beam

proton, the absorbed amplitude in impact parameter space will contain

$$\begin{aligned}\Gamma(\mathbf{r}, \mathbf{b}_V, \mathbf{b}) &= \frac{1}{2} \sigma(\mathbf{r}) t_N(\mathbf{b}_V, B) - \frac{1}{4} \sigma(\mathbf{r}) \sigma_{qq}(\{\mathbf{b}_i\}) t_N(\mathbf{b}_V, B) t_N(\mathbf{b}, B_{el}) \\ &= \Gamma^{(0)}(\mathbf{r}, \mathbf{b}_V) \left( 1 - \frac{1}{2} \sigma_{qq}(\{\mathbf{b}_i\}) t_N(\mathbf{b}, B_{el}) \right) \rightarrow \Gamma^{(0)}(\mathbf{r}, \mathbf{b}_V) \cdot S_{el}(\mathbf{b}).\end{aligned}\quad (2.6)$$

In effect, we merely multiply the Born-level amplitude  $\Gamma^{(0)}$  by the probability amplitude for beam and target to pass through each other without inelastic interaction. In momentum space, we obtain the absorbed amplitude as

$$\begin{aligned}\mathbf{M}(\mathbf{p}_1, \mathbf{p}_2) &= \int \frac{d^2 \mathbf{k}}{(2\pi)^2} S_{el}(\mathbf{k}) \mathbf{M}^{(0)}(\mathbf{p}_1 - \mathbf{k}, \mathbf{p}_2 + \mathbf{k}) \\ &= \mathbf{M}^{(0)}(\mathbf{p}_1, \mathbf{p}_2) - \delta \mathbf{M}(\mathbf{p}_1, \mathbf{p}_2),\end{aligned}\quad (2.7)$$

and with

$$S_{el}(\mathbf{k}) = (2\pi)^2 \delta^{(2)}(\mathbf{k}) - \frac{1}{2} T(\mathbf{k}), \quad T(\mathbf{k}) = \sigma_{tot}^{pp}(s) \exp\left(-\frac{1}{2} B_{el} \mathbf{k}^2\right), \quad (2.8)$$

the absorptive correction  $\delta \mathbf{M}$  reads <sup>3</sup>

$$\delta \mathbf{M}(\mathbf{p}_1, \mathbf{p}_2) = \int \frac{d^2 \mathbf{k}}{2(2\pi)^2} T(\mathbf{k}) \mathbf{M}^{(0)}(\mathbf{p}_1 - \mathbf{k}, \mathbf{p}_2 + \mathbf{k}). \quad (2.9)$$

A number of improvements on this result can be expected to be relevant. Firstly, a more consistent microscopic treatment of spectator interactions along the lines of [22] would be desirable. Experience from hadronic phenomenology [25] suggests that at Tevatron energies, the purely elastic rescattering taken into account by eq.(2.9) are insufficient, and inelastic screening corrections will to a crude estimate lead to an enhancement of absorptive corrections by a factor  $\lambda \sim (\sigma_{el} + \sigma_D)/\sigma_{el}$  [26]. Here  $\sigma_D = 2\sigma_{SD} + \sigma_{DD}$ , and  $\sigma_{SD} = \sigma(pp \rightarrow pX)$ ,  $\sigma_{DD} = \sigma(pp \rightarrow XY)$  are the cross sections for single-, and double-diffractive processes, respectively. Secondly, also the  $\gamma p \rightarrow J/\Psi p$  production amplitude will be affected by unitarity corrections. For example, with increasing rapidity gap  $\Delta y$  between  $J/\Psi$  and the target, one should account for additional  $s$ -channel gluons, and for sufficiently dense multiparton systems, the two-gluon exchange approximation for the  $\gamma \rightarrow J/\Psi$  transition used above, ultimately becomes inadequate. For relevant discussions of unitarity/saturation-effects in diffractive  $J/\Psi$ -production, see [27], the scaling properties of vector meson production in the presence of a large saturation scale are found in [20]. In our present approach, where the production amplitude is taken essentially from experiment, one must content oneself with the fact, that (some) saturation effects are effectively contained in our parametrization, and any extrapolation beyond the energy domain covered by data must be taken with great caution.

### III. RESULTS

In this section we shall present results of differential cross sections for  $J/\Psi$  production. We shall concentrate on the Tevatron energy  $W = 1960 \text{ GeV}$ , where such a measurement might

---

<sup>3</sup> In the practical calculations below, for Tevatron energies, we take  $\sigma_{tot}^{p\bar{p}} = 76 \text{ mb}$ ,  $B_{el} = 17 \text{ GeV}^{-2}$  [24].

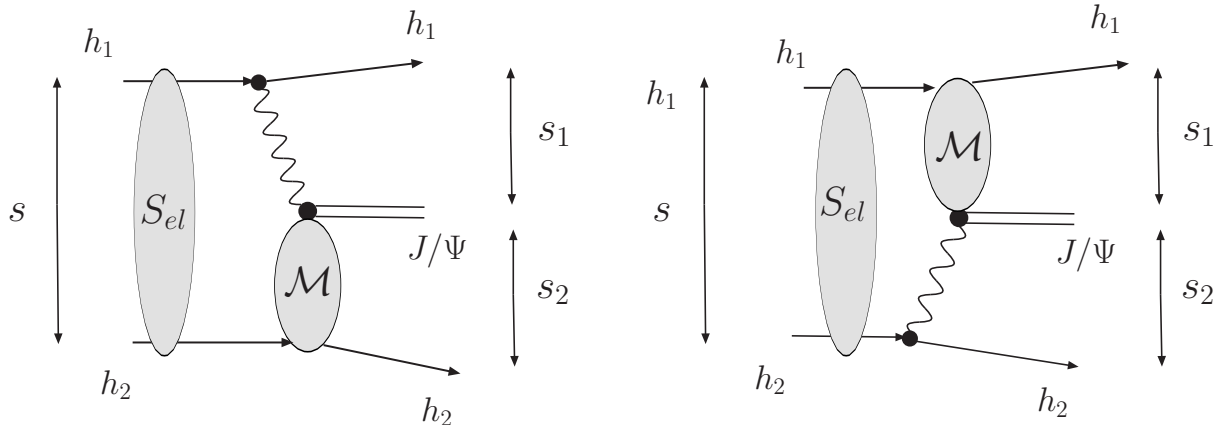


FIG. 3: A sketch of the elastic rescattering amplitudes effectively taken into account by eq.(2.7).

be possible even at present. While in this paper we concentrate on the fully exclusive process  $pp \rightarrow ppJ/\Psi$ ,  $p\bar{p} \rightarrow p\bar{p}J/\Psi$ , it is important to realize, that from an experimental point of view there are additional contributions related to the exclusive production of  $\chi_c$  mesons and their subsequent radiative decays to  $J/\Psi\gamma$ . It may be difficult to measure/resolve the soft decay photons and therefore experimentally this contribution may be seen as exclusive production of  $J/\psi$ . We note in this context that besides the scalar  $\chi_c(0^{++})$  meson, which exclusive production has been discussed in the literature (e.g. [6] and references therein), the axial-vector and tensor states  $\chi_c(1^{++})$  and  $\chi_c(2^{++})$  have larger branching fractions into the relevant  $J/\Psi\gamma$  channel. Although their exclusive production cross sections can be expected to be suppressed at low transverse momenta [6, 28], a more detailed numerical analysis is not existing in the literature and would clearly go beyond the scope of the present paper.

### A. Distributions of $J/\psi$

Let us start from the rapidity distribution of the  $J/\Psi$  shown in Fig.4. In the figure we present also the subsystem energies  $\sqrt{s_1}$ ,  $\sqrt{s_2}$ . At  $|y| > 3$  the energies of the  $\gamma p \rightarrow J/\psi p$  or  $\gamma\bar{p} \rightarrow J/\psi\bar{p}$  subprocesses exceed the energy range explored at HERA. This may open a possibility to study  $J/\Psi$  photoproduction at Tevatron. This is interesting by itself and requires further detailed studies. In turn, this means that our estimate of the cross section far from midrapidity region requires extrapolations above the measured energy domain. In Fig.5 we collect rapidity distributions for different energies relevant for RHIC, Tevatron and LHC. We observe an occurrence of a small dip in the distribution at midrapidity at LHC energy. The shape of the rapidity distribution at LHC energies however relies precisely on the above mentioned extrapolation of the parametrization of HERA-data to higher energies. Clearly a real experiment at Tevatron and LHC would help to constrain cross sections for  $\gamma p \rightarrow J/\psi p$  process.

In order to understand the origin of the small dip at midrapidity at LHC energy in Fig.6 we show separately the contributions of the two components ( $\gamma\mathbf{P}$ ,  $\mathbf{P}\gamma$  exchange) for Tevatron (left) and LHC (right). We see that at LHC energy the two components become better separated in rapidity. This reflects the strong rise of the  $J/\Psi$  photoproduction cross section with energy, which can be expected to slow down with increasing energy. Notice that the beam hadron  $h_1$  moves along positive rapidities, so that, for example for the mechanism

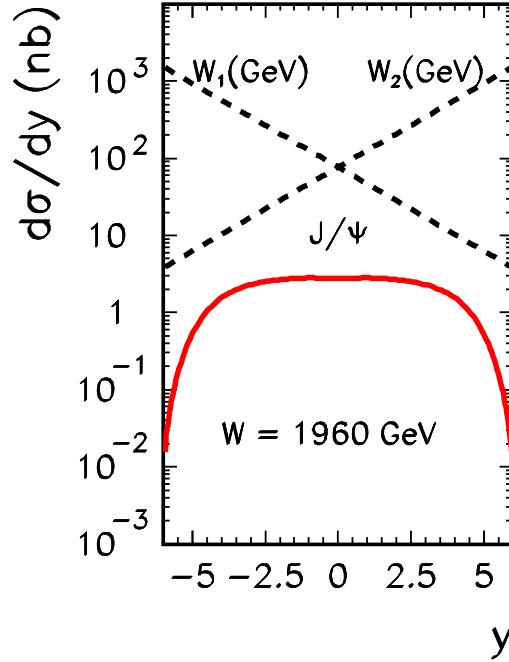


FIG. 4:  $d\sigma/dy$  as a function of the  $J/\Psi$  rapidity ( $y$ ) for  $W = 1960$  GeV. For a better understanding of the results we also show (dashed lines) the subsystem energies  $W_{1V} = \sqrt{s_1}$  and  $W_{2V} = \sqrt{s_2}$  in GeV.

$\gamma\mathbf{IP}$  it is the Pomeron exchange which ‘propagates’ over the larger distance in rapidity space. It would be interesting to confront our present simple predictions with the predictions of the approach which uses unintegrated gluon distributions – objects which are/were tested in other high-energy processes. This will be a subject of our forthcoming studies.

Up to now we have not taken into account any restrictions on  $t_1$  and/or  $t_2$ . In practice, it can be necessary to impose upper cuts on the transferred momenta squared. It is also interesting in the context of searches for odderon, to see how quickly the cross section for the “background” drops with  $t_1$  and  $t_2$ . In Fig.7 we show distribution in  $J/\psi$  rapidity for different cuts on  $t_1$  and  $t_2$ . Clearly, imposing a cut on  $t_1$  and  $t_2$  removes the photon-pole contribution dominant at small momentum transfers. Even relatively small cut lowers the cross section considerably, and the dropping of the cross section is much faster than for the pomeron-odderon exchanges [12]. Imposing upper cuts on  $t_1$  and  $t_2$  will therefore help considerably to obtain a possible “odderon-enriched” sample. We wish to repeat here that without absorption effects the rapidity distribution of  $J/\psi$  in proton-proton and proton-antiproton collisions are identical.

$$\frac{d\sigma(pp \rightarrow ppJ/\Psi, W)}{dy} = \frac{d\sigma(pp \rightarrow p\bar{p}J/\Psi)}{dy} \quad (3.1)$$

It is interesting to stress in this context that it is not the case for transverse momentum



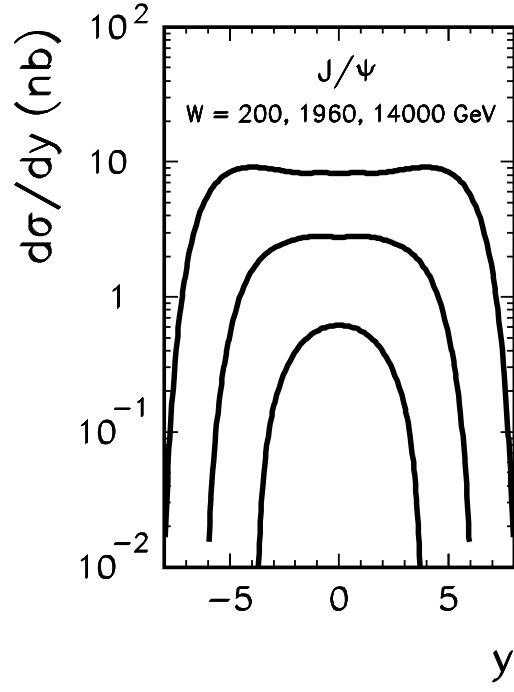


FIG. 5:  $d\sigma/dy$  for exclusive  $J/\psi$  production as a function of  $y$  for RHIC, Tevatron and LHC energies. No absorption corrections were included here.

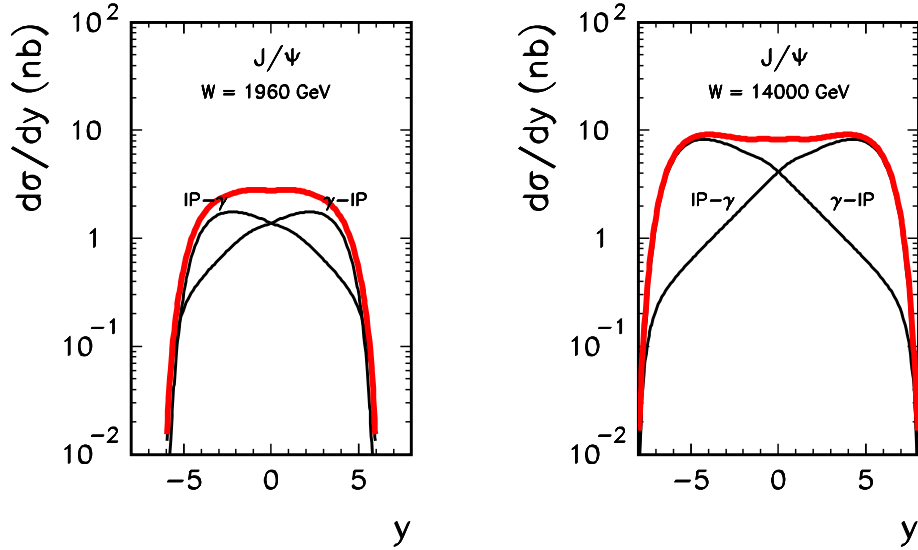


FIG. 6:  $d\sigma/dy$  as a function of  $y$  for the Tevatron and LHC energy. Individual processes are shown separately. Notice that the beam hadron  $h_1$  of Fig. 1 moves at positive rapidities. No absorption corrections were included here.

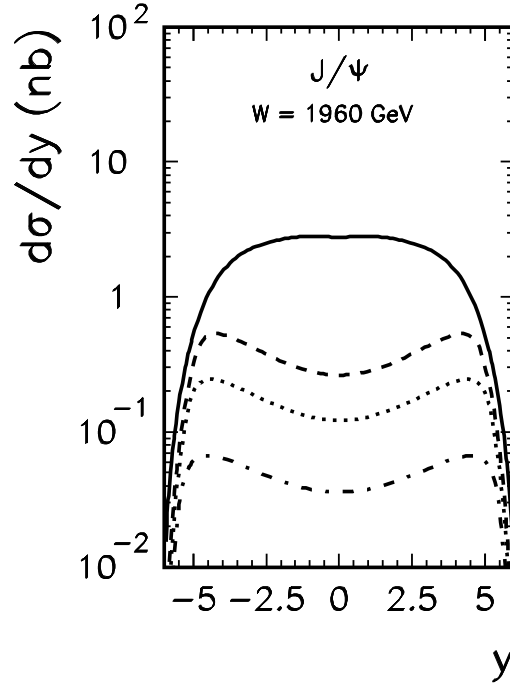


FIG. 7:  $d\sigma/dy$  as a function of  $y$  for the Tevatron energy and different upper cuts on  $t_1$  and  $t_2$ :  $t_{cut} = 0.0 \text{ GeV}^2$  (solid),  $t_{cut} = -0.05 \text{ GeV}^2$  (thin solid),  $t_{cut} = -0.1 \text{ GeV}^2$  (dash-dotted), and  $t_{cut} = -0.2 \text{ GeV}^2$  (dashed).

distribution of  $J/\psi$ , where

$$\frac{d\sigma(pp \rightarrow ppJ/\Psi, W)}{d^2\mathbf{p}_V} \neq \frac{d\sigma(p\bar{p} \rightarrow p\bar{p}J/\Psi, W)}{d^2\mathbf{p}_V}. \quad (3.2)$$

This is demonstrated in Fig.8, where we see, that at small transverse momenta of the vector meson, the interference enhances the cross section in  $pp$  collisions and depletes it in  $p\bar{p}$  collisions. It is a distinctive feature of the mechanism discussed here, that vector mesons are produced with very small transverse momenta. The difference between proton-antiproton and proton-proton collisions survives even at large rapidities of  $J/\psi$ . When integrated over the  $J/\psi$  transverse momentum, and in absence of absorptive corrections, cross sections will again be identical in the  $pp$  and  $p\bar{p}$  cases.

## B. Distributions of (anti-)protons

Now we shall proceed to distributions related to (anti-)protons. In Fig.9 we show distributions in the transferred momenta squared (identical for  $t_1$  and  $t_2$ ). We show separately the contributions of  $\gamma\mathbf{P}$  and  $\mathbf{P}\gamma$  exchanges. The figures clearly display the strong photon-pole enhancement at very small  $t$ .

In order to better understand the distributions in  $t_1$  or  $t_2$  in Fig.10 we show how  $t_1$  and  $t_2$  are correlated. Here we do not make any restrictions on the rapidity range. The significant

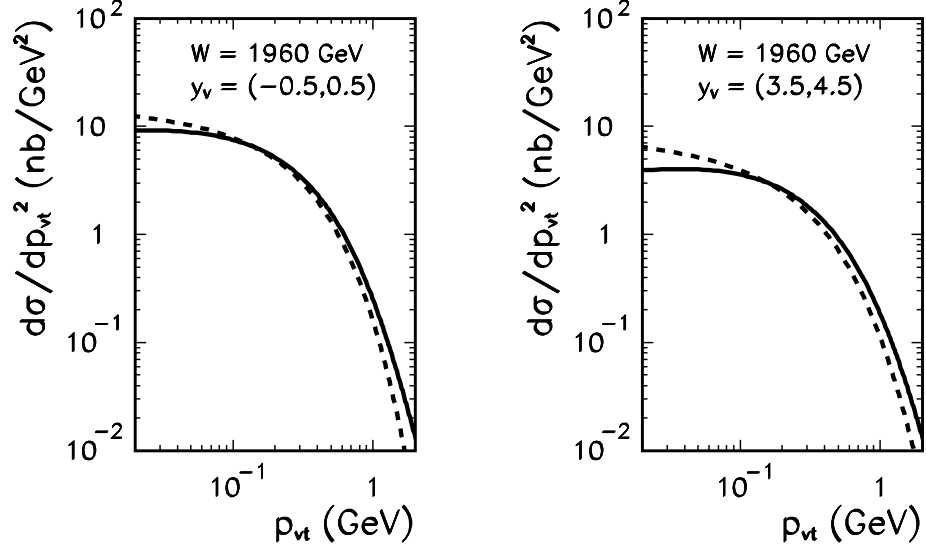


FIG. 8: The distribution  $d\sigma/dp_t^2$  of  $J/\psi$  as a function of  $J/\psi$  transverse momentum for different intervals of rapidity:  $-0.5 < y < 0.5$  (left panel) and  $3.5 < y < 4.5$  (right panel) at  $W = 1960$  GeV. The result for  $p\bar{p}$  collisions is shown by the solid line and the result for  $pp$  collisions by the dashed line. No absorption corrections were included here.

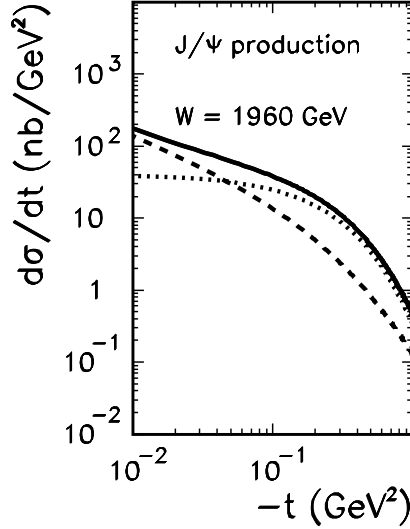


FIG. 9:  $d\sigma/dt_{1/2}$  as a function of Feynman  $t_{1/2}$  for  $W = 1960$  GeV. The photon-exchange (dashed) and pomeron-exchange (dotted) contributions are shown in addition. No absorption corrections were included.

enhancements of the cross section in the form of ridges along  $t_1 \sim 0$  and  $t_2 \sim 0$  are again due to the massless photon-exchange, and most of the integrated cross section comes from these regions. The pomeron-odderon and odderon-pomeron exchange contributions considered in Ref.[12] would not exhibit such a significant local enhancements and would be smeared over broader range in the  $(t_1, t_2)$  space. Therefore in the dedicated searches for the odderon exchange upper cuts on  $t_1$  and  $t_2$  should be imposed, and  $t_{upper} = -0.2$  GeV seems to be a good choice.

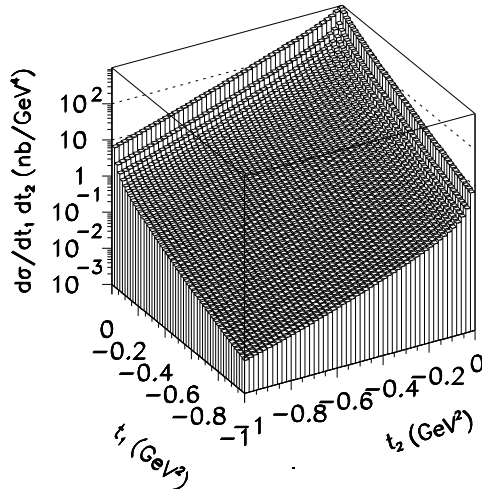


FIG. 10: Two-dimensional distribution in  $t_1$  and  $t_2$  for the Tevatron energy  $W = 1960$  GeV. In this calculation a full range of the  $J/\psi$  rapidities was included. No absorption corrections were included here.

We repeat that the reaction considered in this paper leads to azimuthal correlations between outgoing proton and antiproton. In Fig.11 we show the corresponding angular distribution for proton-antiproton collision (solid line). For reference we also show, by the dotted line, the incoherent sum of the  $\gamma \mathbf{IP}$  and  $\mathbf{IP} \gamma$  mechanisms. The distribution for proton-proton collisions (dashed line) is shown for comparison also at the Tevatron energy. Clearly the interference terms in both reactions are in opposite phase due to different electric charges of proton and antiproton. In the absence of absorptive corrections, we have

$$\frac{d\sigma}{d\phi} = A \pm B \cos \phi \quad (3.3)$$

for  $pp$  (+) and  $p\bar{p}$  (-) collisions respectively. The interference effect ( $B/A$ ) here is at the level of  $\sim 40$ – $50$  %.

In Fig.12 we show the two-dimensional distributions differentially in both rapidity and azimuthal angle. Interestingly, the interference effect is significant over broad range of  $J/\psi$  rapidity, which is reflected in the fact that even at large  $J/\psi$  rapidities one observes anisotropic distributions in the azimuthal angle.

Up to now we have considered only spin-preserving contributions. Now we wish to show the effect of electromagnetic spin-flip discussed in the previous section. In Fig.13 we show the ratio of helicity-flip to helicity-preserving contribution. The ratio is a rather flat function of  $t_1$  and  $t_2$ . At  $t_1 = -1$  GeV<sup>2</sup> and  $t_2 = -1$  GeV<sup>2</sup> the ratio reaches about 0.4.

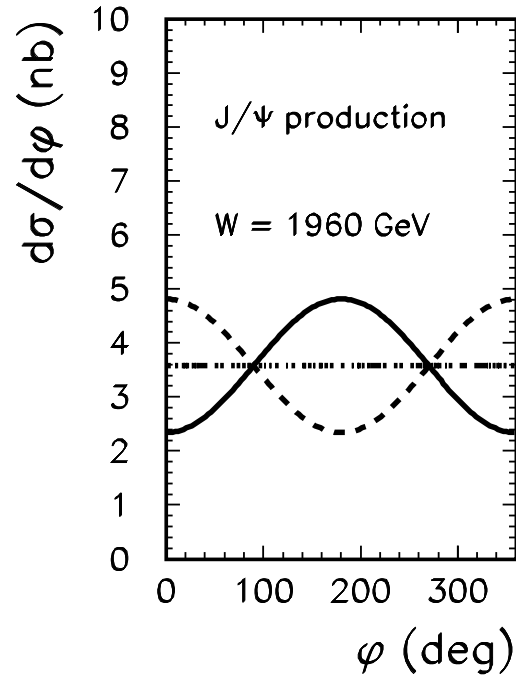


FIG. 11:  $d\sigma/d\phi$  as a function of  $\phi$  for  $W = 1960$  GeV. The solid line corresponds to a coherent sum of amplitudes whereas the dashed line to incoherent sum of both processes. No absorption corrections were included here.

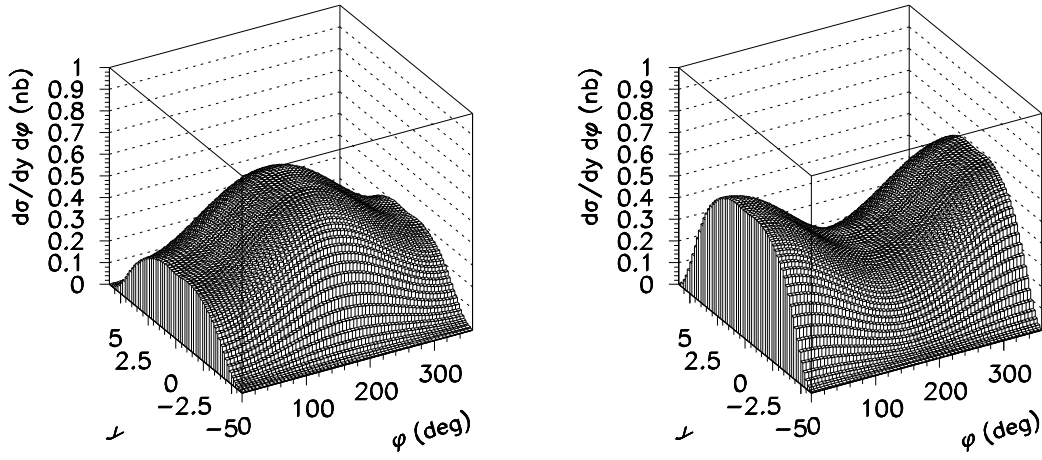


FIG. 12:  $d\sigma/dy d\phi$  for  $W = 1960$  GeV and for  $p\bar{p}$  (left panel) and  $pp$  (right panel) collisions. No absorption corrections were included here.

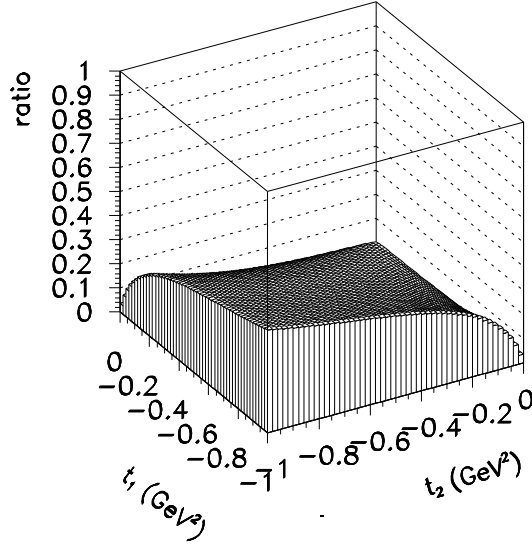


FIG. 13: The ratio of helicity-flip to helicity-preserving contribution as a function of  $t_1$  and  $t_2$ .

### C. Absorption effects

Now we will show the effect of absorptive corrections discussed in section II B on various differential distributions.

Let us start from the presentation of the effects of absorption for selected points in phase space. In Fig.14 we show the fully differential cross section  $d\sigma/dydt_1dt_2d\phi$  as a function of  $\phi$  for selected (fixed) values of  $t_1$ ,  $t_2$  and for  $y = 0$ . We show results for  $p\bar{p}$  (left panel) and  $pp$  (right panel) collisions for the same center-of-mass energy  $W = 1960$  GeV. While at smaller  $t_{1,2}$  we observe a smooth reduction of the Born-level result, absorptive corrections induce a strong  $\phi$ -dependence at larger  $t_{1,2}$ . The positions of the diffractive minima which appear as a consequence of cancellations of the Born and rescattering amplitudes move with the value of  $t \equiv t_1 = t_2$ . In Fig.15 we present fully differential cross section as a function of  $t_1$  and  $t_2$  for  $y=0$  and  $\phi = \pi/2$ . For proton-proton scattering we observe clearly a diffractive minimum for  $t_1 = t_2 \approx 0.4$  GeV<sup>2</sup>. In Fig. 16 we show the fully differential cross section as a function of the transverse momentum squared  $\mathbf{p}_1^2$  at a fixed value  $\mathbf{p}_2^2 = 1$  GeV<sup>2</sup> at rapidity  $y = 0$ . The rich structure as a function of transverse momenta and azimuthal angles is also revealed by this plot. The plots in Fig.17 give an idea, to which extent the diffractive dip-bump structure depends on the details of our treatment of absorption. Here we show, by the dotted line, the cross section calculated for the Born-level amplitude. The solid line shows the result with elastic scattering included, and for the dashed and dash-dotted lines we enhanced the rescattering amplitude  $T$  of section II B by a factor  $\lambda = 1.2$  and  $\lambda = 1.5$  respectively. The region of very small  $\mathbf{p}_1^2$  is entirely insensitive to rescattering, reflecting the ultraperipheral nature of photon exchange. The diffractive dip-bump structure, situated at larger transverse momenta reveals a dependence on the strength of absorptive corrections. This concerns the position of dips as well as the strength of the cross section in various windows of phase space.

The sensitivity to rescattering is however washed out in integrated observables – clearly

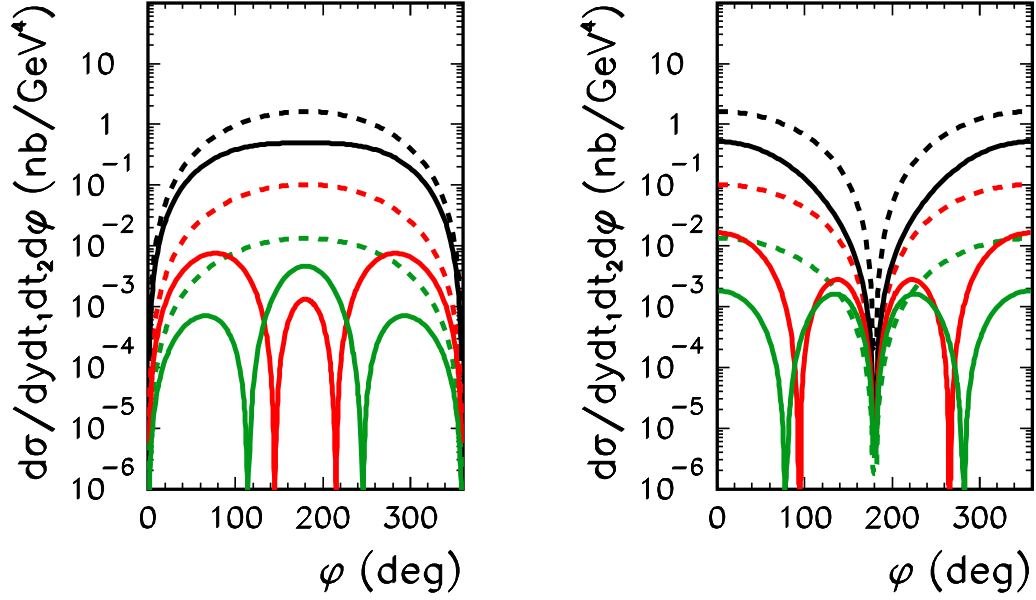


FIG. 14: Fully differential cross section  $d\sigma/dydt_1dt_2d\phi$  as a function of  $\phi$  for  $y=0$  and different combinations of  $t_1 = t_2$  ( $-0.1, -0.3, -0.5$   $\text{GeV}^2$  (from top to bottom)) for  $p\bar{p}$  (left panel) and  $pp$  (right panel) reactions. The solid lines include rescattering, while the dashed lines correspond the Born-level mechanism only.

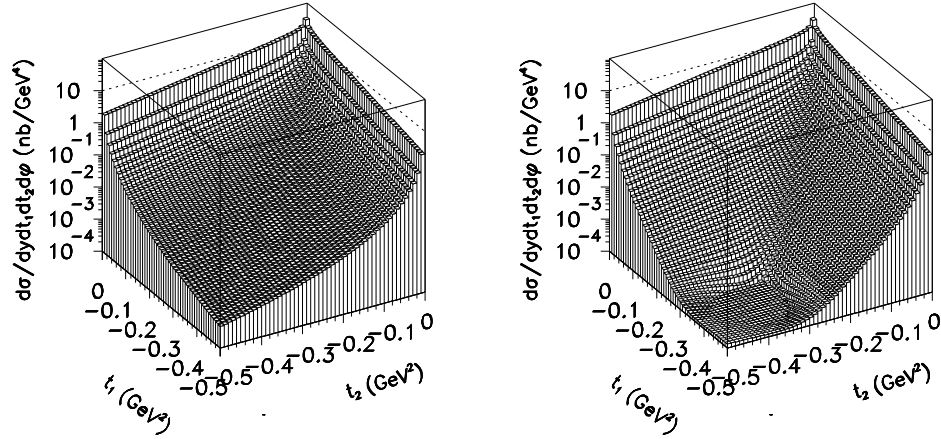


FIG. 15: The fully differential cross section  $d\sigma/dydt_1dt_2d\phi$  as a function of  $t_1$  and  $t_2$  for  $y=0$  and  $\phi = \pi/2$  for  $p\bar{p}$  (left panel) and  $pp$  (right panel) reactions.

the contribution from low transverse momenta, which is not strongly affected by rescattering, is large. This becomes apparent in Figs. 18, 19 and 20.

In Fig.18 we show the ratio of the cross section with absorption to that without absorption as a function of  $t_1$  and  $t_2$ , again for  $p\bar{p}$  (left) and  $pp$  (right). As a consequence of averaging

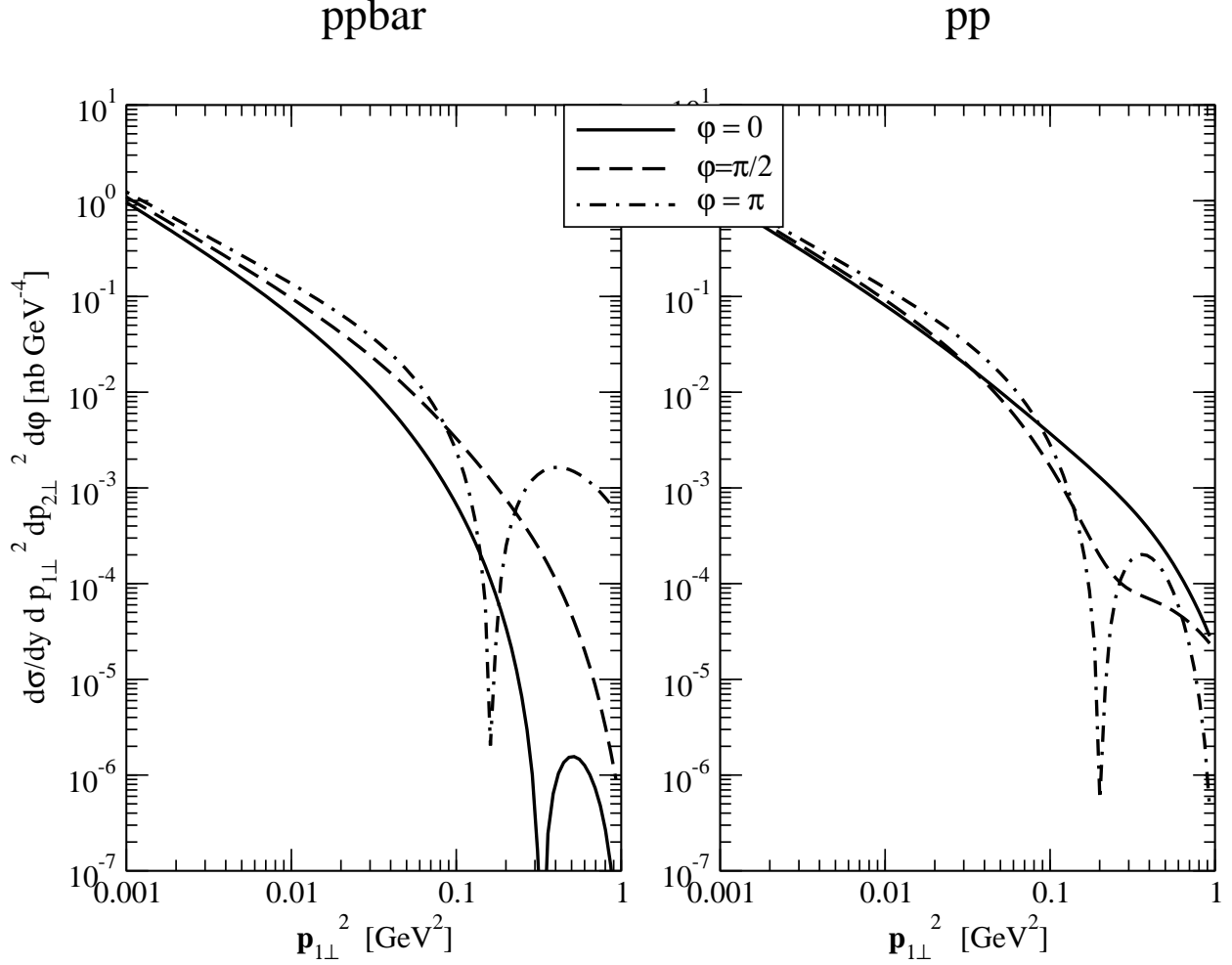


FIG. 16: Fully differential cross section  $d\sigma/dy d p_{1\perp}^2 d p_{2\perp}^2 d\phi$  as a function of  $p_{1\perp}^2$  at  $y = 0$  and  $p_{2\perp}^2 = 1 \text{ GeV}^2$  for  $p\bar{p}$  (left panel) and  $pp$  (right panel) collisions at  $W = 1960 \text{ GeV}$ . Absorptive corrections (elastic rescattering) are included. Solid, dashed, and dash-dotted lines refer to different values of the azimuthal angle  $\phi$  between outgoing (anti-)protons.

over different phase-space configurations the diffractive minima disappeared. Again the plot reflects, that due to the ultraperipheral nature of the photon-exchange mechanism, absorption is negligible at very small  $t_{1,2}$ , and rises with  $t_1$  and/or  $t_2$ . On average, absorption for the  $p\bar{p}$  reaction is smaller than for the  $pp$  case.

It is important to stress again, that the absorptive corrections in differential cross sections cannot be accounted for by simply a constant suppression factor, but show a lively dependence over phase space. In Fig. 19 we show the differential cross section  $d\sigma/dt$ . The dashed line shows the result without absorption, the solid lines include absorptive corrections. They differ by a factor 1.5, by which rescattering had been enhanced in the lower curve. This enhancement of rescattering shows a modest effect, quite in agreement with the expectation mentioned above. The dependence of absorption on  $t$  is quantified by the ratio of full and Born-level cross sections shown by the dotted lines.



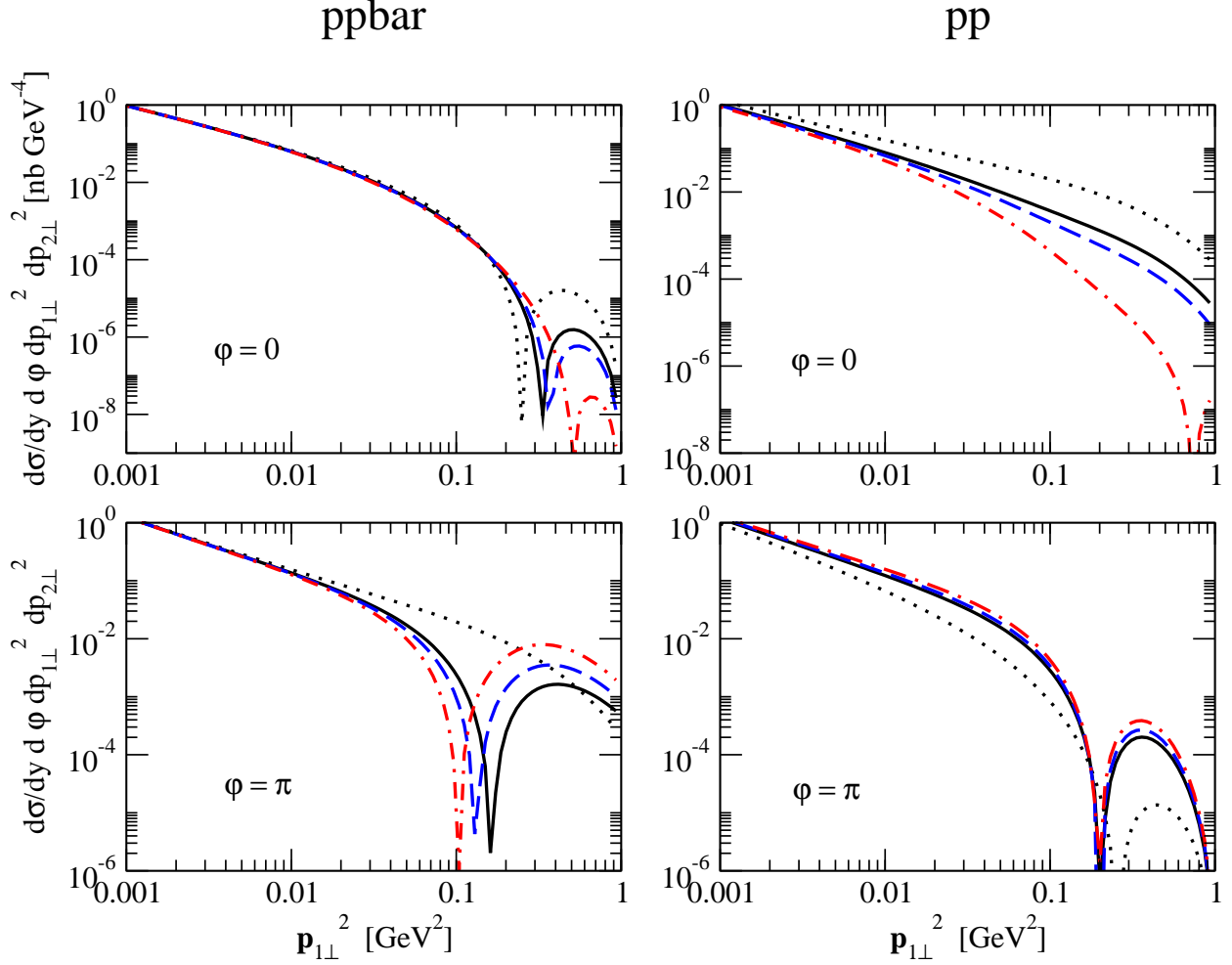


FIG. 17: Fully differential cross section  $d\sigma/dy d\mathbf{p}_1^2 d\mathbf{p}_2^2 d\phi$  as a function of  $\mathbf{p}_1^2$  at  $y = 0$  and  $\mathbf{p}_2^2 = 1\text{GeV}^2$  for  $p\bar{p}$  (left panel) and  $pp$  (right panel) collisions at  $W = 1960$  GeV. The azimuthal angle  $\phi$  is taken  $\phi = 0$  in the top row and  $\phi = \pi$  in the second row. Shown by the dotted curve is the Born-level cross section, without absorptive corrections included. The solid curve shows the result with elastic rescattering between (anti-) protons included, while rescattering has been enhanced by a factor  $\lambda = 1.2$  in the amplitude for the dashed curve, and by a factor  $\lambda = 1.5$  for the dash-dotted curve.

In Fig. 20 we show the suppression factor

$$\langle S^2(\mathbf{p}_V^2) \rangle = \frac{d\sigma^{\text{Born+Rescatt.}}/d\mathbf{p}_V^2 dy}{d\sigma^{\text{Born}}/d\mathbf{p}_V^2 dy}, \quad (3.4)$$

as a function of the  $J/\Psi$  transverse momentum at  $y = 0$ . It is important to emphasize once more the strong functional dependence on  $\mathbf{p}_V$ , which is different for  $p\bar{p}$  and  $pp$  collisions. Again, playing with the strength of absorptions shows a modest effect.

The different behaviour of absorptive corrections in  $pp$  and  $p\bar{p}$  collisions is an interesting observation. It derives from the fact that rescattering corrections lift the cancellation of the interference term after azimuthal integration. Finally, let us comment on the expected reduction of rapidity distributions from absorptive corrections. These are, finally, rather flat

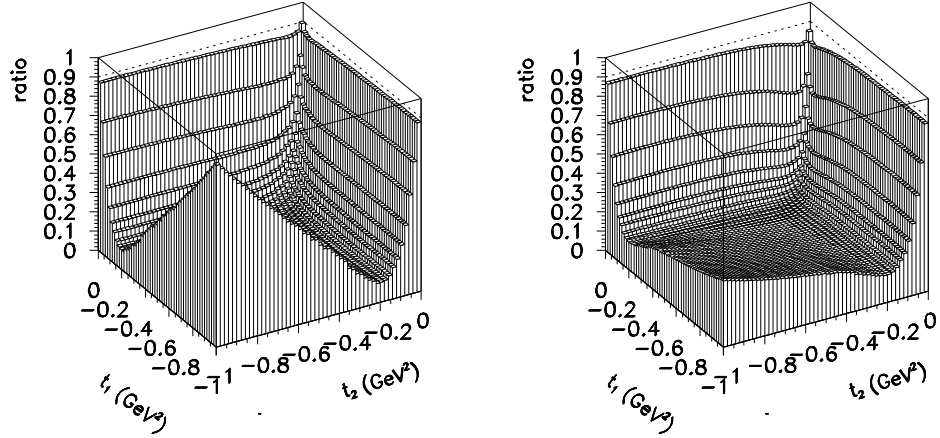


FIG. 18: The ratio of the cross sections with absorption to that without absorption for  $p\bar{p}$  (left panel) and  $pp$  (right panel) scattering. Here the integration over  $y$  and  $\phi$  was performed.

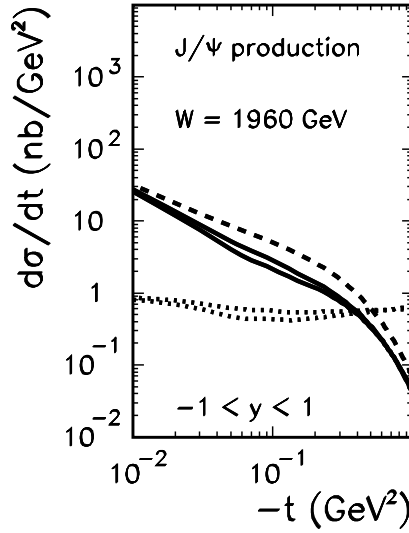


FIG. 19: Differential cross section  $d\sigma/dt$ , integrated over  $-1 < y < 1$  for  $p\bar{p}$  collisions. Dashed line: no absorptive corrections. Solid lines show the cross section with absorptive corrections included. Upper solid line: purely elastic rescattering. Lower solid line: rescattering enhanced by a factor  $\lambda = 1.5$  in the amplitude. The dotted lines show the respective ratios  $d\sigma^{\text{Born+Rescatt.}}/d\sigma^{\text{Born}}$ .

functions of  $y$ . For the ratio

$$\langle S^2(y) \rangle = \frac{d\sigma^{\text{Born+Rescatt.}}/dy}{d\sigma^{\text{Born}}/dy}, \quad (3.5)$$

we obtain, in  $p\bar{p}$  collisions

$$\langle S^2(y=0) \rangle \Big|_{p\bar{p}} \approx 0.9, \quad \langle S^2(y=3) \rangle \Big|_{p\bar{p}} \approx 0.8, \quad (3.6)$$

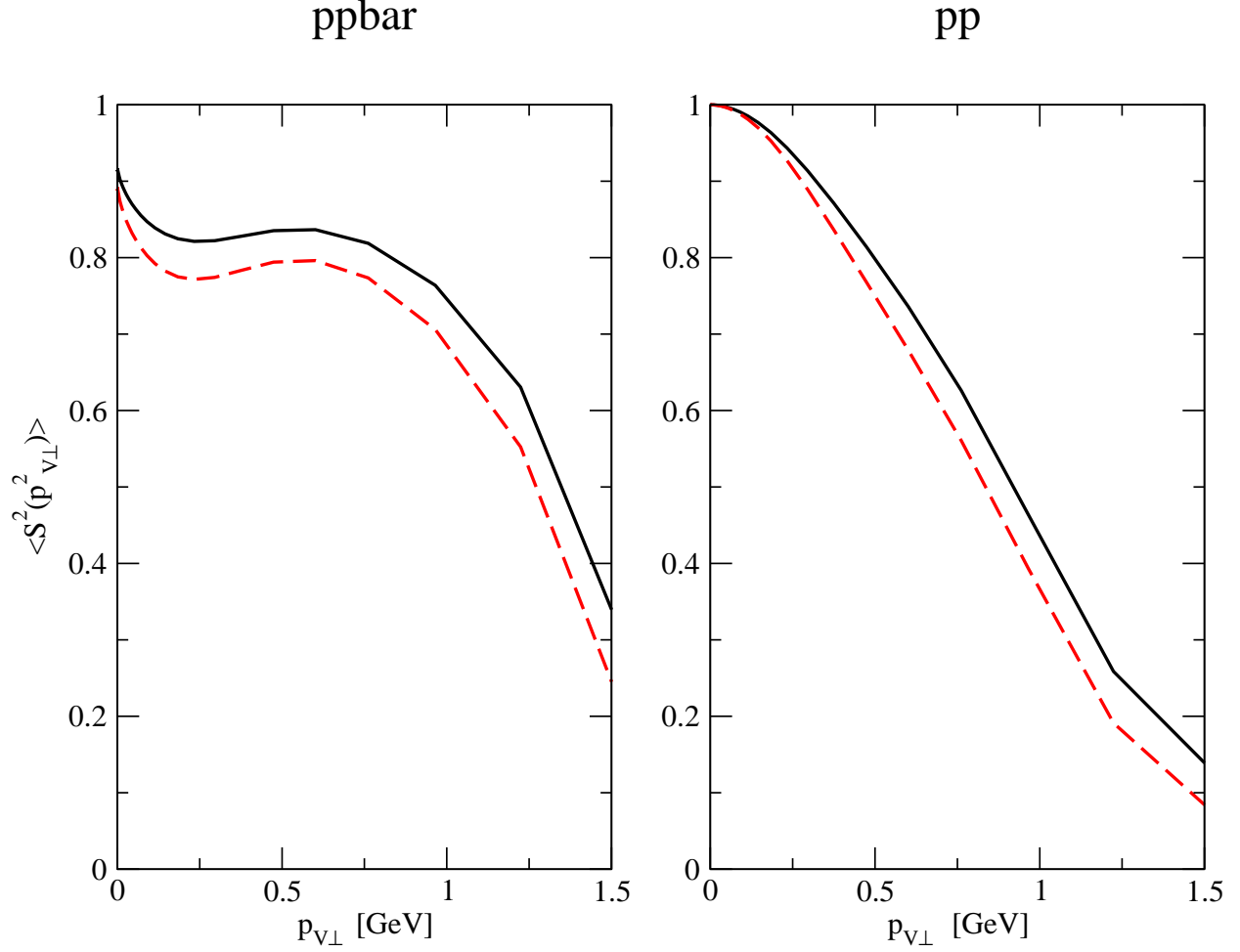


FIG. 20: The suppression factor  $\langle S^2(\mathbf{p}_{V\perp}^2) \rangle$  at  $y = 0$  as a function of the  $J/\Psi$  transverse momentum, for  $p\bar{p}$  (left panel) and  $pp$  (right panel) collisions at  $W = 1960$  GeV.

and for  $pp$  collisions

$$\langle S^2(y = 0) \rangle \Big|_{pp} \approx 0.85, \quad \langle S^2(y = 3) \rangle \Big|_{pp} \approx 0.75. \quad (3.7)$$

We note that this results in a small charge asymmetry

$$\frac{d\sigma(p\bar{p})/dy - d\sigma(pp)/dy}{d\sigma(p\bar{p})/dy + d\sigma(pp)/dy} \approx 2 \div 3 \%, \quad (3.8)$$

which derives entirely from absorptive corrections.

#### IV. CONCLUSIONS

In this paper we have calculated differential cross sections for exclusive  $J/\psi$  production via photon-pomeron( $\gamma\mathbf{P}$ ) and pomeron-photon ( $\mathbf{P}\gamma$ ) exchanges at RHIC, Tevatron and LHC energies. Measurable cross sections were obtained in all cases. We have obtained an interesting azimuthal-angle correlation pattern due to the interference of the  $\gamma\mathbf{P}$  and  $\mathbf{P}\gamma$

mechanisms. The interference effect survives over almost the whole range of  $J/\psi$  rapidities. At the Tevatron energy one can potentially study the exclusive production of  $J/\psi$  at the photon-proton center-of-mass energies  $70 \text{ GeV} < W_{\gamma p} < 1500 \text{ GeV}$ , i.e. in the unmeasured region of energies, much larger than at HERA. At LHC this would be correspondingly  $200 \text{ GeV} < W_{\gamma p} < 8000 \text{ GeV}$ . At very forward rapidities this is an order of magnitude more than possible with presently available machines. Due to the photon-pole, the differential cross section is concentrated in the region of very small  $t_1$  or/and  $t_2$ . Imposing cuts on  $t_1$  and  $t_2$  lowers the cross section considerably. Electromagnetic helicity-flip processes play some role only when both  $|t_1|$  and  $|t_2|$  are large, that is in a region where also the hypothetical hadronic, Odderon exchange, contribution can be present. It is a distinctive feature of the production mechanism, that mesons are produced at very small transverse momenta, where the interference of  $\gamma\mathbf{IP}$  and  $\mathbf{IP}\gamma$  mechanisms induces a strongly different shape of vector-meson  $\mathbf{p}_{V-}^2$  distributions in  $pp$  vs.  $p\bar{p}$  collisions. We also estimated absorption effects on various distributions. In some selected configurations the absorptive corrections lead to the occurrence of diffractive minima. Naturally, the exact place of diffractive minima depends on the values of the model parameters, but they are washed out when integrated over the phase space or even its part. Absorptive corrections for differential distributions are lively functions of transverse momenta, and cannot be accounted for simply by constant suppression factors. We have found that absorptive corrections induce a small charge-asymmetry in rapidity distributions and total production cross sections. In the present paper we have concentrated on exclusive production of  $J/\psi$  at energies  $\sqrt{s} > 200 \text{ GeV}$ . The formalism used here can be equally well applied to exclusive production of other vector mesons, such as  $\phi$ ,  $\Upsilon$  as well as to the lower energies of e.g. FAIR, J-PARC, RHIC. For  $J/\psi$ -production, especially recent parametrizations [29] of the photoproduction cross section from threshold to the highest energies may prove useful. We leave such detailed analyses for separate studies. The processes considered here are also interesting in the context of recently proposed searches for identifying the Odderon. We find that the region of midrapidities ( $-1 < y < 1$ ) and  $t_1, t_2 < -0.2 \text{ GeV}^2$  seems the best in searches for the odderon exchange. Should data reveal deviations from the conservative predictions given by us, a detailed differential analysis of both, photon and odderon-exchange processes, including their interference, in  $y, t_1, t_2, \phi$  will be called upon.

## V. ACKNOWLEDGMENTS

We thank Mike Albrow for useful comments regarding the experimental possibilities of exclusive  $J/\Psi$ -production at the Tevatron. We are indebted to Tomasz Pietrycki for help in preparing some figures. This work was partially supported by the grant of the Polish Ministry of Scientific Research and Information Technology number 1 P03B 028 28.

## VI. APPENDIX

In Ref.[2] the differential cross section  $\frac{d\sigma}{dt}$  for the reaction  $\gamma^*p \rightarrow J/\psi p$  was parametrized as

$$\frac{d\sigma}{dt}(W, t, Q^2) = \frac{d\sigma}{dt}\Big|_{t=0, W=W_0} \left(\frac{W}{W_0}\right)^{4(\alpha(t)-1)} \exp(B_0 t) \left(\frac{m_{J/\psi}^2}{m_{J/\psi}^2 + Q^2}\right)^n, \quad (6.1)$$

where  $\alpha(t) = \alpha_0 + \alpha' t$ . The values of parameters found from the fit to the data are:  $\frac{d\sigma}{dt}|_{t=0, W=W_0} = 326 \text{ nb/GeV}^2$ ,  $W_0 = 95 \text{ GeV}$ ,  $B_0 = 4.63 \text{ GeV}^{-2}$ ,  $\alpha_0 = 1.224$ ,  $\alpha' = 0.164 \text{ GeV}^{-2}$ ,  $n = 2.486$ .

Assuming the dominance of the helicity-conserving transitions, and neglecting the real part, one can write

$$\mathcal{M}(s, t, Q^2) = \delta_{\lambda_\gamma \lambda_V} \delta_{\lambda_p \lambda_{p'}} i s \sqrt{16\pi \frac{d\sigma}{dt}|_{t=0, W=W_0}} \left( \frac{s}{W_0^2} \right)^{\alpha(t)-1} \exp(B_0 t/2) \left( \frac{m_{J/\psi}^2}{m_{J/\psi}^2 + Q^2} \right)^{n/2}, \quad (6.2)$$

identical for each combination of particle helicities. In our case of hadroproduction the amplitude is a function of either  $(s_1, t_1, Q_2^2)$  or  $(s_2, t_2, Q_1^2)$ .

- 
- [1] S. Chekanov *et al.* [ZEUS Collaboration], Eur. Phys. J. C **24**, 345 (2002).
  - [2] A. Aktas *et al.* [H1 Collaboration], Eur. Phys. J. C **46**, 585 (2006).
  - [3] I. Ivanov, N.N. Nikolaev and A.A. Savin, Phys. Part. Nucl. **37** 1 (2006).
  - [4] D. Barberis *et al.* [WA102 Collaboration], Phys. Lett. B **440** 225 (1998); Phys. Lett. B **432**, 436 (1998); Phys. Lett. B **427**, 398 (1998); Phys. Lett. B **397**, 339 (1997); Phys. Lett. B **488**, 225 (2000).
  - [5] F.E. Close, G.R. Farrar and Z. Li, Phys. Rev **D55** 5749 (1997); N.I. Kochelev, T. Morii and A.V. Vinnikov, Phys. Lett. **B457** 202 (1999); F.E. Close and G.A. Schuler, Phys. Lett. **B464** 279 (1999); A. B. Kaidalov, V. A. Khoze, A. D. Martin and M. G. Ryskin, Eur. Phys. J. C **31**, 387 (2003).
  - [6] V.A. Khoze, A.D. Martin, M.G. Ryskin and W.J. Stirling, Eur. Phys. J. **C35** 211 (2004).
  - [7] R. Pasechnik, A. Szczurek and O. Teryaev, a paper in preparation.
  - [8] A. Szczurek, R. Pasechnik and O. Teryaev, Phys. Rev. **D75** 054021 (2007).
  - [9] V.A. Khoze, A.D. Martin and M.G. Ryskin, Phys. Lett. **B401** 330 (1997);
  - [10] M. Boonekamp, A. De Roeck, R. Peschanski and C. Royon, Phys. Lett. B **550**, 93 (2002); C. Royon, Acta Phys. Polon. B **37**, 3571 (2006).
  - [11] A. Schäfer, L. Mankiewicz and O. Nachtmann, Phys. Lett. **B272** 419 (1991).
  - [12] A. Bzdak, L. Motyka, L. Szymanowski and J.-R. Cudell, Phys. Rev. D **75**, 094023 (2007).
  - [13] V.A. Khoze, A.D. Martin and M.G. Ryskin, Eur. Phys. J. **C23** 311 (2002).
  - [14] S.R. Klein and J. Nystrand, Phys. Rev. Lett. **92** 142003 (2004); V. P. Goncalves and M. V. T. Machado, Eur. Phys. J. C **40**, 519 (2005).
  - [15] N. N. Nikolaev, Comments Nucl. Part. Phys. **21**, 41 (1992).
  - [16] J. D. Bjorken, Phys. Rev. D **47**, 101 (1993).
  - [17] B. Z. Kopeliovich, J. Nemchick, N. N. Nikolaev and B. G. Zakharov, Phys. Lett. B **309**, 179 (1993); B. Z. Kopeliovich, J. Nemchick, N. N. Nikolaev and B. G. Zakharov, Phys. Lett. B **324**, 469 (1994).
  - [18] N. N. Nikolaev and B. G. Zakharov, Z. Phys. C **49**, 607 (1991).
  - [19] J. Nemchik, N. N. Nikolaev, E. Predazzi, B. G. Zakharov and V. R. Zoller, J. Exp. Theor. Phys. **86**, 1054 (1998) [Zh. Eksp. Teor. Fiz. **113**, 1930 (1998)].
  - [20] I. P. Ivanov, N. N. Nikolaev and W. Schäfer, Phys. Part. Nucl. **35**, S30 (2004).
  - [21] V. A. Abramovsky, V. N. Gribov and O. V. Kancheli, Yad. Fiz. **18** (1973) 595 [Sov. J. Nucl. Phys. **18** 308 (1974)]; A. Capella and A. Kaidalov, Nucl. Phys. B **111** 477 (1976); L. Bertocchi

- and D. Treleani, J. Phys. G **3**, 147 (1977).
- [22] N. N. Nikolaev and W. Schäfer, Phys. Rev. D **74**, 074021 (2006).
  - [23] V. N. Gribov, Sov. Phys. JETP **29**, 483 (1969) [Zh. Eksp. Teor. Fiz. **56**, 892 (1969)].
  - [24] F. Abe *et al.* [CDF Collaboration], Phys. Rev. D **50**, 5518 (1994).
  - [25] B. Z. Kopeliovich, N. N. Nikolaev and I. K. Potashnikova, Phys. Rev. D **39**, 769 (1989).
  - [26] K. A. Ter-Martirosyan, Sov. J. Nucl. Phys. **10**, 600 (1970) [Yad. Fiz. **10**, 1047 (1969)].
  - [27] H. Kowalski and D. Teaney, Phys. Rev. D **68**, 114005 (2003); H. Kowalski, L. Motyka and G. Watt, Phys. Rev. D **74**, 074016 (2006); M. Kuroda and D. Schildknecht, Phys. Lett. B **638**, 473 (2006).
  - [28] F. Yuan, Phys. Lett. B **510**, 155 (2001).
  - [29] R. Fiore, L.L. Jenkovszky, V.K. Magas, F. Paccanoni and A. Prokudin, Phys. Rev. D **75**, 116005 (2007).